

Easy preparation of novel 3,3-dimethyl-3,4-dihydro-2H-1,2,4-benzothiadiazine 1,1-dioxide: Molecular structure, Hirshfeld surface, NCI analyses and molecular docking on AMPA receptors

Koffi Sénam Etsè^{a,*}, Guillermo Zaragoza^b, Kodjo Djidjolé Etsè^c

^a Laboratory of Medicinal Chemistry, Center for Interdisciplinary Research on Medicines (CIRM), University of Liège, Quartier Hôpital B36 Av. Hippocrate 15 B-4000 Liège, Belgium

^b Unidad de Difracción de Raios X, RIAIDT, Universidad de Santiago de Compostela, Campus VIDA, 15782 Santiago de Compostela, Spain

^c Laboratoire de Physiologie et Biotechnologie Végétales (LPBV), Faculté des Sciences (FDS), Université de Lomé (UL), Lomé, Togo

ARTICLE INFO

Article history:

Received 6 February 2021

Revised 22 March 2021

Accepted 2 April 2021

Available online 10 April 2021

Keywords:

Benzothiadiazine 1,1-dioxide

X-ray molecular structures

Hirshfeld surface

NCI plot

Molecular docking

AMPA receptors

ABSTRACT

We present in this study the synthesis and characterization of a new 3,3-dimethyl-substituted 1,2,4-benzothiadiazine 1,1-dioxide. 3,3-dimethyl-3,4-dihydro-2H-1,2,4-benzothiadiazine 1,1-dioxide **10**, was obtained by reacting 2-aminobenzenesulfonamide with acetone. The molecular structures of the starting sulfonamide and the new benzothiadiazine were obtained by X-ray diffraction analysis and the interactions like hydrogen bonds stabilizing the crystal packing were discussed. The contacts are confirmed by non-covalent interaction analysis. Analyses of Hirshfeld surface mapped over d_i , d_e , d_{norm} and shape-index were further used to identify the intermolecular interactions. The fingerprint histogram allow to show that H...H (45.7%) and O...H (30.1%) contacts are the dominant interactions in the crystal packing of **10**. The effects of the molecular environment were accessed by analyzing the electron density isosurface and the 3D-topology of energy frameworks. The prediction of physicochemical properties suggested that **10** could be considered as a lead-like drug. Therefore, molecular docking study was performed on the α -amino-3-hydroxy-5-methyl-4-isoxazolepropionic acid receptor (AMPA) and suggested that **10** could interact with the allosteric site located on the ligand binding domain of AMPAR and could be a positive allosteric modulator. Docking results show that **10** can bind in a symmetrical way in the GluA2 ligand binding domain with two molecules at the dimer interface. The results also demonstrated that the presence of two methyl groups at the 3-position of the thiadiazine ring induced rotation of **10** in the binding site leading to close contacts with Pro494, Ser497, Ser729 and Ser754.

© 2021 Elsevier B.V. All rights reserved.

1. Introduction

Learning and cognition pathology, attention disorders in children, senile dementias, brain disorders, Parkinson and Alzheimer disease are becoming serious problem in global public health. Studies have proven that enhancement of α -amino-3-hydroxy-5-methyl-4-isoxazolepropionic acid (AMPA) signals by compounds known as AMPAR potentiators could be beneficial in the management of these neurological disorders pathologies [1–3]. Indeed, various research groups have become interested in AMPA receptors (AMPARs) and shown that upregulation of these receptors could produce cognition enhancement [4]. The modulatory activity of

AMPA positive allosteric modulators (AMPApams) derive from the fact that when binding with the ligand-binding domain (LBD), positive allosteric modulators stabilize the receptor in its open state and therefore slowing the deactivation and/or the desensitization processes, or induce conformational modification leading to the closure of the channel [5–8].

Since Bertolino and coworkers discovered the potency of IDRA21 (**1**) as an AMPAR-pam [9], a great number of ring fused thiadiazine derivatives were synthesized and tested as new AMPAR potentiators. In the thiadiazine family, 1,2,4-benzothiadiazine 1,1-dioxides (BTDs) were revealed as the most potent AMPAR-pams [10]. Among known AMPAR-pam BTDs, cyclothiazide (**2**), BPAM344 (**3**), BPAM538 (**4**) and **5** were shown to be highly potent (Fig. 1) [11–14]. In order to develop novels more potent therapeutics, pharmacomodulation studies continued to propose various structures.

* Corresponding author.

E-mail address: ks.ets@uliege.be (K.S. Etsè).

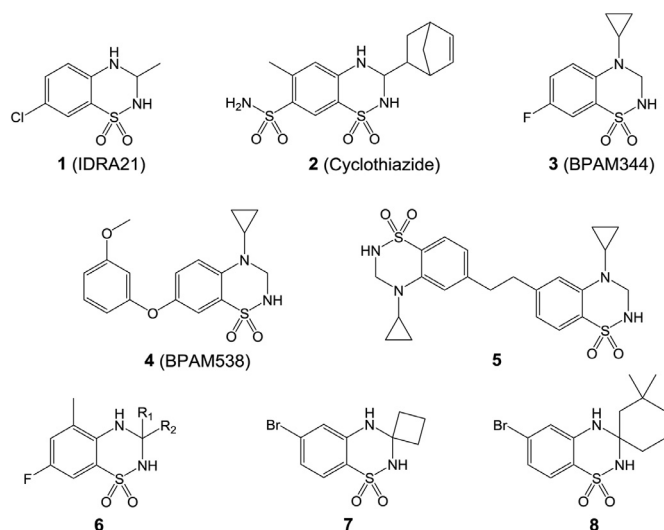


Fig. 1. Chemical structures of selected AMPAR potentiators (**1–5**) and selected 3,3-dialkyl-substituted 1,2,4-benzothiadiazine 1,1-dioxides (**6–8**).

The structure/activity relationships, in particular the effect and the position of substituents on the benzothiadiazine ring was discussed by Chamberlin et al. [15]. Although the activities of **6** derivatives by varying the R1 and R2 groups are discussed, the activity of derivatives without substituent on the benzyl ring at 5 and 7 positions were not reported. Except with few examples, little is known about the molecular structure impact and physicochemical properties of BTDs bearing two alkyl groups at the 3-position and the real impact of such modification on biological property and activity.

3,3-disubstituted BTDs molecular structures are the less described in BTD derivatives. Despite the crystal structures of compounds **7** and **8** (Fig. 1) are recently briefly reported, their other properties and biological potentiality remains to be explored [16]. Molecular structure determination has emerged as an interesting way to describe three dimensional architecture, steric effects and bonds orientation behaviors of compounds. Data from the molecular structure could be used to explain or predict some physical properties and biochemical activities [17–19]. Therefore, structure activity studies is a good way to identify structural suitability of promising drug candidates and to reduce the number of costly failures experiments.

As part of an ongoing project on BTD-type compounds, 3,3-dimethyl-3,4-dihydro-2H-1,2,4-benzothiadiazine 1,1-dioxide (**10**) was synthesized. The present work aims the full characterization of the new BTD and that of its precursor 2-aminobenzenesulfonamide. The characterization is completed by the three dimensional molecular structure determination thanks to X-ray diffraction analyses. All the interactions present in the crystal structures and the energies stabilizing the crystal packing of these compounds will be deeply analyzed. The prediction of some important physicochemical parameters like toxicity mutagenic, tumorigenic, irritant and reproductive effective as well as screening for their drug score and drug-likeness will be discussed. Furthermore, a docking study will be realized in order to assess the plausible binding mode of the new BTD as a putative AMPAR-pam. Particular attention will be paid in analyzing the influence on the binding mode of the presence of two methyl groups at the 3-position of the benzothiadiazine ring.

2. Experimental

The syntheses were realized using standard Schlenk techniques. For characterization, ^1H , and ^{13}C NMR spectra were recorded at

298 K using a Bruker DRX NMR spectrometer operating at 500 and 126 MHz, respectively. Chemical shifts were quoted in parts per million (δ) downfield from TMS and were referenced from the residual solvent peaks or TMS [20]. Spin multiplicities are indicated by the following symbols: s (singlet), d (doublet), t (triplet) and m (multiplet). The coupling constants, J , are reported in Hertz (Hz).

2.1. Synthesis and crystallization

Synthesis of 2-aminobenzenesulfonamide **9**.

2-Aminobenzenesulfonamide was obtained from Aldrich Belgium or prepared according to the method previously developed by Girard starting from aniline [21]. NMR analysis was performed to check the purity (See supporting information). Monocrystals of **9** suitable for X-ray diffraction analysis were obtained after one week at 6 °C of a slow evaporation of its solution in a mixture of acetone/dichloromethane (2/5).

Synthesis of 3,3-dimethyl-3,4-dihydro-2H-1,2,4-benzothiadiazine 1,1-dioxide **10**.

The title compound was obtained by stirring 2-aminobenzenesulfonamide **9** (350 mg) in 20 ml of acetone at room temperature during 48 h. The starting light orange mixture turned into a colorless solution. The conversion was followed by tin layer chromatography. After completion of the reaction, the excess of acetone was removed by evaporation under reduced pressure, and the solid residue obtained was purified by silica gel column chromatography with a mixture of dichloromethane/ethyl acetate (5/1) as the eluent. The product was isolated as a colorless crystalline solid. Yield: 93%. R_f (dichloromethane/ethyl acetate in 5/1): 0.63. M.p.: 152–154 °C. ^1H NMR (500 MHz, $\text{DMSO}-d_6$) δ 7.57 (s, 1H), 7.43 (d, $J = 8.0$ Hz, 1H), 7.25 (t, $J = 8.0$ Hz, 1H), 7.03 (s, 1H), 6.71 (d, $J = 8.0$ Hz, 1H), 6.67 (t, $J = 8.0$ Hz, 1H), 1.48 (s, 6H). ^{13}C NMR (126 MHz, $\text{DMSO}-d_6$) δ 142.83, 132.78, 132.72, 123.76, 123.67, 115.94, 68.46, 28.35. Anal. calcd. for $\text{C}_9\text{H}_{12}\text{N}_2\text{O}_2\text{S}$: C, 50.93; H, 5.70; N, 13.20; S, 15.10. Found: C, 50.89; H, 5.75; N, 13.14; S, 15.18%.

Suitable monocrystals of **10** for X-ray diffraction analysis were obtained after two weeks at 6 °C of a slow evaporation of its solution in a mixture of acetone/dichloromethane (2/5).

2.2. Single crystal X-ray diffraction data collection

For the crystal structure determination, the previously reported procedure was used [22]. Briefly, the data were collected by applying the omega and phi scans method on a Bruker D8 Venture PHOTON III-14 diffractometer using INCOATEC multilayer mirror monochromated with $\text{MoK}\alpha$ radiation ($\lambda = 0.71073$ Å) for compound **9** and $\text{CuK}\alpha$ ($\lambda = 1.54060$ Å) for compound **10** from a microfocus sealed tube source at 100 K. Computing data and reduction were made with the APEX3 [23]. The structure was solved using SHELXT [24] and finally refined by full-matrix least-squares based on F^2 by SHELXL [25]. An empirical absorption correction was applied using the SADABS program. Software used to molecular graphics: ORTEP for Windows [26]. Software used to prepare material for publication: WinGX publication routines [26] and Mercury [27].

Crystal data, data collection and structure refinement details are summarized in Table 1. All non-hydrogen atoms were refined anisotropically and the hydrogen atom positions were included in the model on the basis of Fourier difference electron density maps. All CH and aromatic CH hydrogen ($\text{C}-\text{H} = 0.95$ Å) atoms were refined using a riding model with $\text{Uiso}(\text{H}) = 1.2$ Ueq(C). The methyl hydrogen ($\text{C}-\text{H} = 0.98$ Å) atoms were refined as a rigid group with torsional freedom [$\text{Uiso}(\text{H}) = 1.5$ Ueq(C)]. The H atoms positions and isotopic atomic factors of amine groups were refined as a free atoms.

Table 1
Crystal data and details of the structure refinement for compounds **9** and **10**.
Experimental details.

Crystal data	Compound 9	Compound 10
Chemical formula	C ₆ H ₈ N ₂ O ₂ S	C ₉ H ₁₂ N ₂ O ₂ S
M _r	172.2	212.27
Crystal system	Monoclinic	Monoclinic
Space group	P2 ₁ /c	P2 ₁ /n
Temperature (K)	100	100
a (Å)	8.4370 (12)	7.2235 (7)
b (Å)	9.1483 (13)	9.8674 (8)
c (Å)	10.0274 (15)	14.3551 (13)
V (Å ³)	732.56 (19)	993.22 (16)
B	108.824 (8)	103.902 (7)
Z	4	4
Radiation type	Mo Kα	Cu Kα
μ (mm ⁻¹)	0.39	2.72
Crystal size (mm)	0.16 × 0.14 × 0.13	0.18 × 0.15 × 0.05
Data collection		
Diffractometer	Bruker D8 VENTURE PHOTON III-14	
Absorption correction	Multi-scan SADABS2016/2 – Bruker AXS area detector scaling and absorption correction	
T _{min} , T _{max}	0.840, 0.874	0.921, 0.971
No. of measured, independent and observed [I > 2σ(I)] reflections	50,965, 3550, 3016	32,755, 1948, 1899
R _{int}	0.064	0.034
(sin θ/λ) _{max} (Å ⁻¹)	0.833	0.617
Refinement	0.033, 0.086, 1.11	0.027, 0.072, 1.03
R[F ² > 2σ(F ²)], wR(F ²), S	116	137
No. of parameters		
H-atom treatment	H atoms treated by a mixture of independent and constrained refinement	
Δρ _{max} , Δρ _{min} (e Å ⁻³)	0.50, -0.44	0.46, -0.37

Crystallographic data for compounds **9** and **10** have been deposited at the Cambridge Crystallographic Data center with the numbers CCDC-2057734 and CCDC-2057733 respectively. These data can be obtained free of charge via <http://www.ccdc.cam.ac.uk/conts/retrieving.html> (or from the Cambridge Crystallographic Data center, 12, Union Road, Cambridge CB2 1EZ, UK; fax: +44 1223 336033).

2.3. Molecular docking studies

To study the binding mode on AMPARs, compound **10** was subjected to protein-ligand interactions. Molecular docking calculations were performed with AUTODOCK 4.2 [28]. The cocrystal structure of BPAM344 with GluA2o-LBD-L504Y-N775S (PDB code 4N07, resolution of 1.87 Å) retrieved from the protein data bank (PDB) was used in the docking study [12]. All the ligand molecules attached to the proteins were removed. All the water molecules were removed, missing hydrogen atoms were added and non-polar hydrogens were merged into their corresponding carbon atoms using AutoDock Tools. A grid box size of 60×60×60 Å³ was defined around the GluA2 LBD. 3D molecular structure of compound **10** obtained from the X-ray crystal structure data was used for the docking. During docking simulation, 20 conformers were first considered by using default genetic algorithm. The docking procedure is further repeated five times. Finally, 100 runs are performed to obtain robust population for the analyses. The poses resulting of the docking calculation are superimposed and reported in Figure S5. Input preparation was done by using MGLTools-1.5.6. Further, the protein processed through AutoDock Tools was used to create PDBQT file and generated the Grid Parameter File (GPF). The grid box parameters also saved in GPF file and the Grid Log File (GLG) was generated by running Autogrid protocol. Then, the Docking Parameter File (DPF) was generated with Lamarckian genetic algorithm by setting the protein as rigid molecule. Finally, the DLG (Docking Log File) file is created by running Autodock with DPF as input file. Using the Autogrid module, the electrostatic and atomic

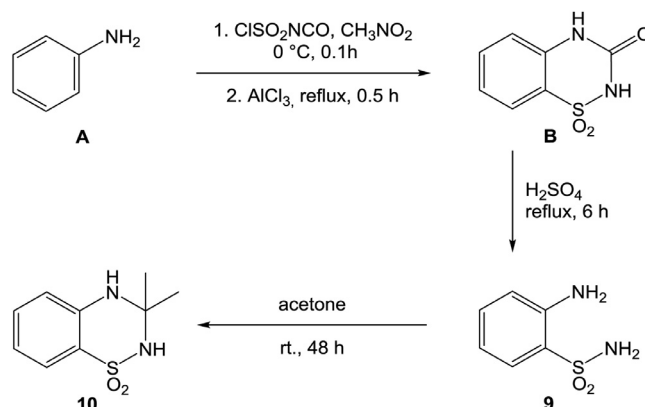


Fig. 2. Synthesis of 3,3-dimethyl-3,4-dihydro-2H-1,2,4-benzothiadiazine 1,1-dioxide **10**.

interaction maps for all atoms of **10** was calculated. Out of several interactions possible, the best pose with lowest binding energy and the most probable was considered for further protein-ligand docking. PyMOL [29] was used for docking conformation representation.

3. Results and discussion

3.1. Synthesis

The synthetic pathways leading to the desired BTD **10** is shown in Fig. 2. The key intermediate 2-aminobenzenesulfonamide (**9**) required for the preparation of the product was obtained starting from aniline. Aniline **A** was reacted first with chlorosulfonyl isocyanate in the conditions described by Girard et al. [21] to obtain 2H-benzo[e][1,2,4]thiadiazin-3(4H)-one 1,1-dioxide **B**. The latter was then hydrolyzed in the presence of 50% sulfuric acid in water to give 2-aminobenzenesulfonamide **9** as a light brown solid that was characterized by NMR analysis and compared to the com-

mercial product. The ^1H NMR spectra recorded in $\text{DMSO}-d_6$ highlights two broad peaks at 7.20 and 5.83 ppm attributed to $\text{C}_{\text{arm}}-\text{NH}_2$ and SO_2-NH_2 protons respectively confirming the formation of the sulfonamide.

To obtain the desired benzothiadiazine dioxide **10**, the experimental conditions developed by Kumar et al. [30] were tried. Indeed, compound **9** was first allowed to react with 1.1 equivalent of acetone in the presence of 1.5 equivalents of magnesium sulfate and polyphosphoric acid anhydride in toluene at 100 °C. Using such procedure, the reaction didn't lead to the product. This result is probably due to the low boiling point of acetone. We then performed the reaction at room temperature during one night. Purification of the reaction mixture highlighted various byproducts associated to the expected benzothiadiazine dioxide in less than 20% yield. Realizing the reaction without polyphosphoric acid anhydride provided an increase of the yield (35%). Finally, the simple reaction of the sulfonamide **9** with acetone used as reactant and solvent in a close flask at room temperature during 48 h was found to be the best conditions with a very good yield of 93% (Fig. 2).

The proton nuclear magnetic resonance spectrum of compound **10** confirms the formation of the desired product. Indeed, the two methyl groups signals appear at 1.48 ppm as a singlet for the six protons. The benzothiazine heterocycle resulting from the ring closure reaction comprises two different N–H bonds. The SO_2-NH proton is observed at 7.57 ppm and the second $\text{C}_{\text{arm}}-\text{NH}$ proton is localized at 7.03 ppm. The chemical shifts for aromatic ring protons were found to be around 6.5–7.5 ppm as a set of doublets and triplets.

3.2. Molecular structures description

In view to complete the compounds characterization, we attempted to obtain monocrystals of **9** and **10** suitable for X-ray diffraction analysis. Fortunately, crystals of these compounds were obtained by slow evaporation of their solution in a mixture of acetone/dichloromethane (2/5) and were further analyzed. The molecular structures of the two compounds were then confirmed unambiguously from the single X-ray diffraction results and the experimental data are reported in Table 1. Other structural and interactions descriptors like NCI plot and Hirshfeld surface were further used to describe the structures.

3.2.1. X-ray structural description of compound 9

The sulfonamide **9** crystallizes in monoclinic $P2_1/c$ space group and the molecular structure is shown in Fig. 3a. The aniline C_6-N_2 and the sulfonamide C_1-S_1 , S_1-N_1 , $\text{S}-\text{O}$ bonds length of 1.3745 (12), 1.7559 (9), 1.6052 (9) and ~ 1.44 Å respectively, are typical of the distances observed in aniline and sulfonamide compounds [31,32]. The dihedral angle $\text{N}_2-\text{C}_6-\text{C}_1-\text{S}_1$ value of 3.27 ° revealed that the aniline and the sulfone bonds are almost coplanar with the aromatic ring. The amine H atoms are implicated on intra and intermolecular interactions. These interactions were therefore analyzed and reported in Fig. 3b. The oxygen O1 linked to the sulfur atom is implicated in one intramolecular hydrogen bond with the H4N hydrogen of the aniline. This interaction is characterized by a $\text{N}_2\cdots\text{O}_1$ distance 2.9517(13) Å and a $\text{N}_2-\text{H}_4\text{N}\cdots\text{O}_1$ angle of 130.9 (16) °.

The analysis of the crystal packing shows that the molecular structure is stabilized by the presence of short intermolecular interactions (Fig. 3b). Each molecule is linked to one another via hydrogen bonds that stabilize the crystal packing of this aminobenzenesulfonamide.

The sulfonamide group is implicated in two different hydrogen bonds: $\text{N}_1-\text{H}_2\text{N}\cdots\text{O}_2^{\text{ii}}$ ($-x, y + 1/2, -z + 1/2$) and $\text{N}_1-\text{H}_2\text{N}\cdots\text{O}_1^{\text{i}}$ ($x, -y + 1/2, z + 1/2$). These interactions are characterized by a $\text{N}_1\cdots\text{O}_2^{\text{ii}}$ distance of 2.9684 (12) Å, similar to $\text{N}_1\cdots\text{O}_1^{\text{i}}$ distance

(2.93017(12) Å). The respective donor–H–acceptor angles are 163.6 (17) ° and 170.0(15) ° (See Table S1). These intermolecular interactions extend as an infinite chain along crystallographic b axis direction (Fig. 3c).

3.2.2. Hirshfeld surface analysis of compound 9

The interactions stabilizing the crystal packing of compound **9** can be also described by analyzing the mapping of various contact descriptors mapped on the Hirshfeld surface using CrystalExplorer17 program [33]. The donors, the acceptors, the withdrawing groups, the hydrogen bonds and $\pi-\pi$ interactions could be visualized and identified on the different surfaces. This strategy is therefore employed to complete all the contacts described earlier. The maps of d_{norm} , d_i and d_e on molecular Hirshfeld surfaces of compound **9** are shown in Fig. 4. A front and back view are present to allow best visualization of the different contacts. The red spots on the surfaces mapped over d_{norm} depicted hydrogen bonding and reveals that the sum of d_i and d_e is shorter than the sum of the Van der Waals radii [34,35].

In 2-aminobenzenesulfonamide **9**, the surface mapped over d_i shows red spots around N1H1 and N1H2 atoms revealing that they are the nearest internal nuclei from the point of the surface. In the other hand, the red spots on the d_e surface show that O1 and O2 atoms of the sulfonamide group are the nearest external nuclei from the point of the surface behaving like acceptor groups in the intermolecular N–H \cdots O interactions in **9**. Hence, the normalized d_{norm} mapped on the Hirshfeld surface confirmed the presence of the two intermolecular $\text{N}_1-\text{H}_1\text{N}\cdots\text{O}_1^{\text{i}}$ and $\text{N}_1-\text{H}_2\text{N}\cdots\text{O}_2^{\text{ii}}$ hydrogen bonds involved in the crystal structure as red spots on the surface. The nearest molecules in the crystal packing implicated in these contacts are shown and the interaction are highlighted as dashed yellow lines on Fig. 4. Finally, the Hirshfeld surface was also mapped with Shape-index. Convex blue regions represent hydrogen donor groups and concave red regions represent acceptor groups. The donor as well as acceptor properties of N1H hydrogens and SO oxygens are confirmed by blue and red spots respectively on the Shape-index surface located around these atoms.

CrystalExplorer software allows characterization of the molecular structure of compound in the crystallographic environment encompassing all the close contacts by the means of plotting the two-dimensional Fingerprint histogram [35,36]. The fingerprint plot indicates the contributions of interatomic contacts to the Hirshfeld surfaces in the crystal packing [37]. The 2D fingerprint plot of 2-aminobenzenesulfonamide and the percentage of contribution of each interaction are presented in Fig. 4(a–j). Decomposed fingerprint of compound **9** reveals that the most important contributions come from O \cdots H (34.6%), H \cdots H (34.2%) and H \cdots C (19.9%) interactions. The percentage of O \cdots H contribution in the fingerprint could be explained by the presence of hydrogen bonds. Other interactions percentages are shown in Fig. 4(e–j).

In view to assess the weight on the interactions energies stabilizing the crystal packing, the various intermolecular interactions energies were calculated using CE-B3LYP/6–31G(d,p) energy model available in CrystalExplorer [38,39]. The resulting interaction energies frameworks are represented graphically as energy diagrams in Fig. 5. A view along the crystallographic a , b and c axes are shown to allow better description. The radii of the corresponding cylinders are proportional to the magnitude of interaction energy. The molecules surrounding the original one indicated in black are color coded according to their interaction energy within a cluster of radius of 3.8 Å in the three dimensions. The total intermolecular energy E_{tot} (kJ/mol) relative to the reference molecule (in black) is obtained by summing the energies of four main components, comprising electrostatic (E_{ele}), polarization (E_{pol}), dispersion (E_{dis}) and exchange-repulsion (E_{rep}) [38] with scale factors of 1.057, 0.740, 0.871 and 0.618, respectively [40,41].

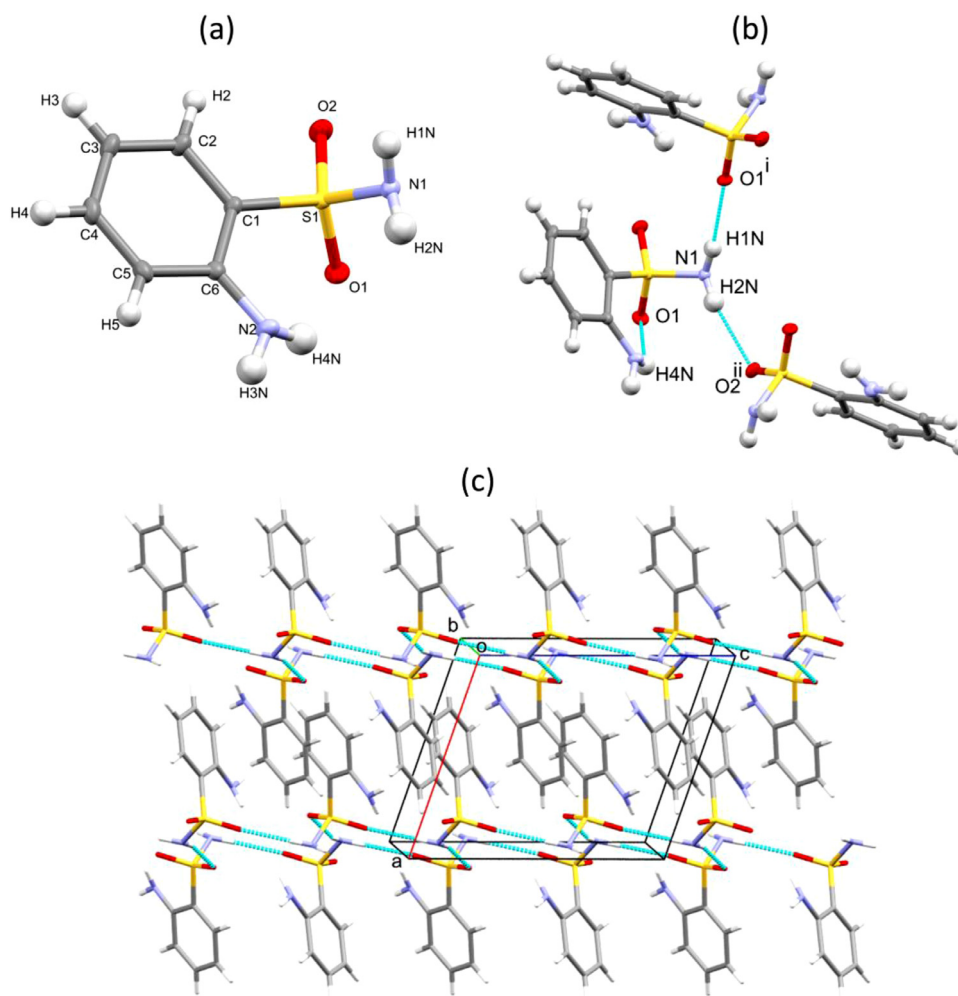


Fig. 3. (a) The molecular structure of compound **9** showing the atom labeling. Displacement ellipsoids are drawn at the 50% probability level. (b) Intramolecular N2–H4N...O1 and intermolecular N1–H1N...O1ⁱ and N1–H2N...O2ⁱⁱ hydrogen bonds present in compound **9**. Symmetry codes: (i) $x, -y + 1/2, z + 1/2$; (ii) $-x, y + 1/2, -z + 1/2$. (c) Packing diagram showing intermolecular hydrogen bonds.

Table 2
Hydrogen-bond geometry in compound **10**.

D–H...A	D–H (Å)	H...A (Å)	D...A (Å)	D–H...A (°)
C8–H8A...O1	0.98	2.6	3.1462 (17)	115
N2–H2N...O1 ⁱ	0.82 (2)	2.18 (2)	2.9857 (15)	169.0 (18)
N1–H1N...O2 ⁱⁱ	0.824 (19)	2.09 (2)	2.9043 (15)	170.8 (17)

Symmetry codes: (i) $-x + 1/2, y + 1/2, -z + 3/2$; (ii) $-x + 1, -y + 1, -z + 1$.

The different energy components are resumed in Table 2S (See supporting information). The total interaction energy value $E_{\text{tot}} = -151.2$ kJ/mol involving the electrostatic (-93.6 kJ/mol), polarization (-28.9 kJ/mol), dispersion (-129.1 kJ/mol) and repulsion (131.7 kJ/mol) was obtained. The molecules color coded in red and orange implicated in the intermolecular hydrogen bonds (N1–H1N...O1ⁱ and N1–H2N...O2ⁱⁱ), gave the highest interaction energies of -29.8 kJ/mol and -49.4 kJ/mol respectively. The lower negative energy value of the molecules color coded in orange is furthermore confirmed by the lowest molecular centroid distance (R) of 5.06 Å.

3.2.3. Structural description of compound **10**

The molecular structure on the 3,3-dimethyl-3,4-dihydro-2H-1,2,4-benzothiadiazine 1,1-dioxide (**10**) was also obtained and shown in Fig. 6. Compound **10** crystallizes instead of **9** in mono-

clinic $P2_1/n$ space group with crystal volume of 993.22 (16) Å³. The C7–N1 [1.4827 (16) Å] and C7–N2 [1.4691 (17) Å] bonds length are in the same order of those obtained for this compound family [30]. The C6–N2 distance observed in the aniline **9** [1.3745 (12) Å] is almost the same to that in benzothiazine **10** [1.3818 (17) Å]. The conformation of the thiadiazine ring (C1–S1–N1–C7–N2–C6) can be evaluated by considering some dihedral angles of the heterocycle. The different torsion angles C7–N1–S1–C1, N2–C7–N1–S1, C6–N2–C7–N1 and C1–C6–N2–C7 values of -39.88 (11), 55.69 (13), -46.14 (16) and 24.88 (19) ° respectively, suggested notable deviation of the carbon atom C7 from the mean plane. Furthermore, the values of Cremer and Pople [42] parameters giving puckering amplitude $Q = 0.4118(13)$ Å, $\theta = 42.27(18)$ ° and $\Phi = 94.5(2)$ ° strongly suggested that the C1–S1–N1–C7–N2–C6 ring adopts an envelope conformation.

The crystal structure and the molecular packing of the compound **10** are stabilized by the existence of hydrogen bonds. As a consequence of tetragonal geometry around the carbon C7, one hydrogen atom bearing to exocyclic C8 carbon is therefore oriented toward one oxygen of the sulfonamide group leading to intramolecular interaction. Such interaction is observed between H8A and O1 and reported in Fig. 6. Data of hydrogen bonds are resumed in Table 2. The crystal packing is stabilized by the presence of two hydrogen bonds established between the N–H atoms and oxygen atoms of two different neighboring molecules. The bonds

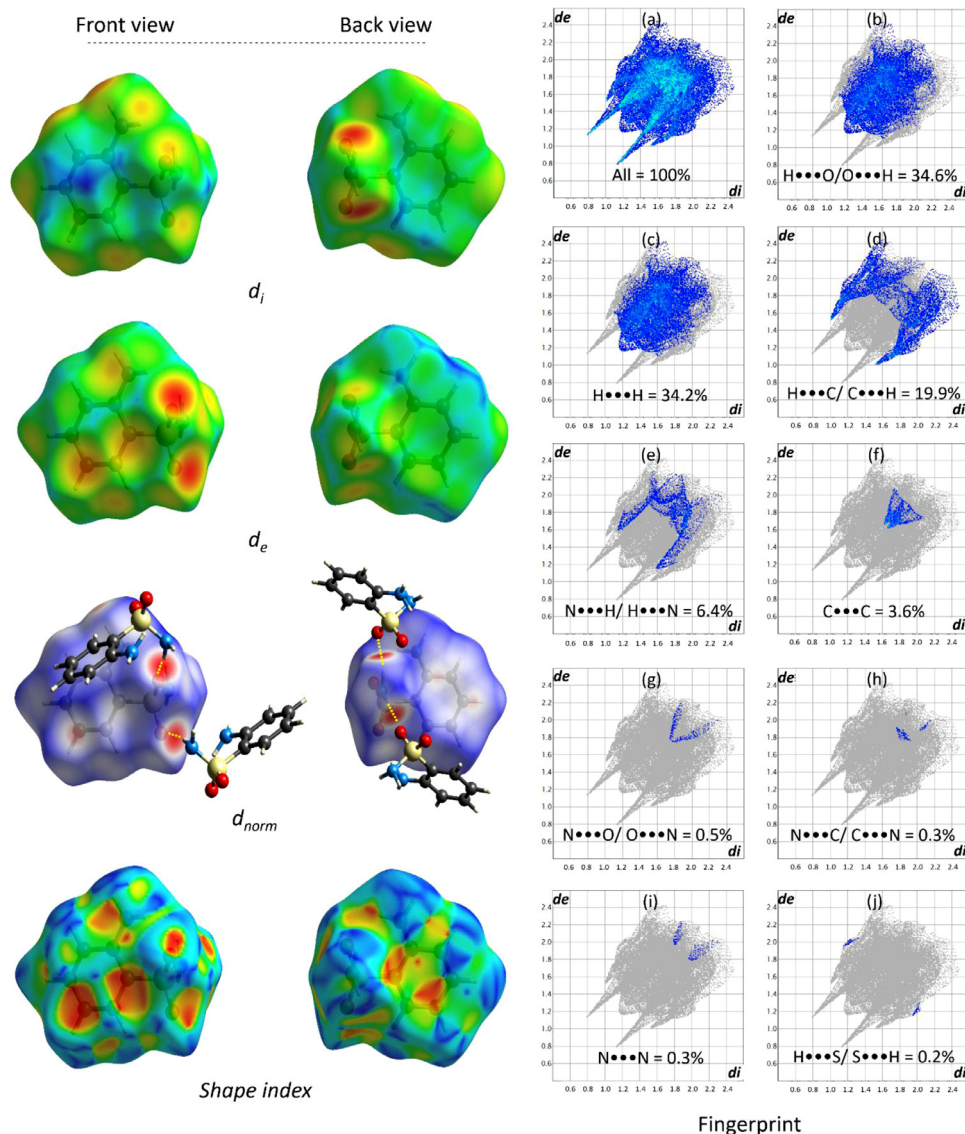


Fig. 4. The Hirshfeld surface of the sulfonamide **9** mapped over d_i in the range 0.7962 to 2.4898 Å, d_e in the range 0.7978 to 2.4656 Å, d_{norm} in the range -0.5205 to 1.0610 and shape-index (-1.0 to 1.0). The two-dimensional fingerprint plots of compound **9** and the decomposed contribution (a-j).

distances and angles characterizing these intermolecular interactions are almost the same (Table 2). The representation of these hydrogen bonds in the crystal packing formed a grid as shown in Fig. 7a.

Further, stabilization of the crystal packing is ensured by $X-H\cdots\pi$ interactions. The disposition of the molecules in the crystal packing induces proximity of C9–H9A hydrogen of each molecule with the π electrons of the adjacent molecule phenyl ring Cg (C1→C6). The intermolecular $X-H\cdots\pi$ interactions in the crystal packing are presented in Fig. 7b. Such interaction parameters were measured based on the method described by Malone et al. [43] giving values of H9A...Cg = 2.644 Å, H–Perp = 2.604 Å and C9...Cg = 3.547 Å. The value of the angle formed by [C9–H9A– π] named α is 153.3° suggesting that the hydrogen atom H9A almost pointed towards the center of the π ring Cg. Furthermore, the H9A atom is practically above the Cg center confirmed by $\theta = 80.7^\circ$.

3.2.4. Hirshfeld surface analysis of BTD 10

The interactions described earlier are furthermore analyzed by examining the Hirshfeld surface and are shown in Fig. 8. The Hir-

shfeld surfaces of two sides were also shown to description fluency. The red spots observed on d_i , d_e surfaces correspond to the $N-H\cdots O$ (d_i) and $O\cdots H-N$ (d_e) strong contacts. Furthermore, the presence of round yellow spots surrounded by a black circle on d_i and d_e confirmed the presence of $X-H\cdots\pi$ contact. The three-dimensional d_{norm} surface was mapped over a fixed color -0.5418 (red) to 1.4079 (blue) highlighting intermolecular $O\cdots H$ close contacts as red spots. The interactions are highlighted as yellow dash line and are shown in Fig. 8. The white and blue regions on the d_{norm} surface reveal distances equal and longer than the sum of the Van der Waals radii respectively with the nearest molecules. The deep red spots attributed to hydrogen bonds revealed that these interactions are much strong interactions than $X-H\cdots\pi$ contacts (white spots) (Fig. 8). In addition to the acceptor (red region) and donor (blue region) groups observed on Hirshfeld surface mapped over Shape-index, the $X-H\cdots\pi$ interaction is clearly identified as concave red region and the contact molecule is presented. There are no regions with adjacent red and blue triangles on the Shape index map indicating a lack of $\pi\cdots\pi$ interactions in the crystal packing. The $X-H\cdots\pi$ interactions can further be visualized on the curvedness plots of compound **10** (Fig. 8). Curvedness

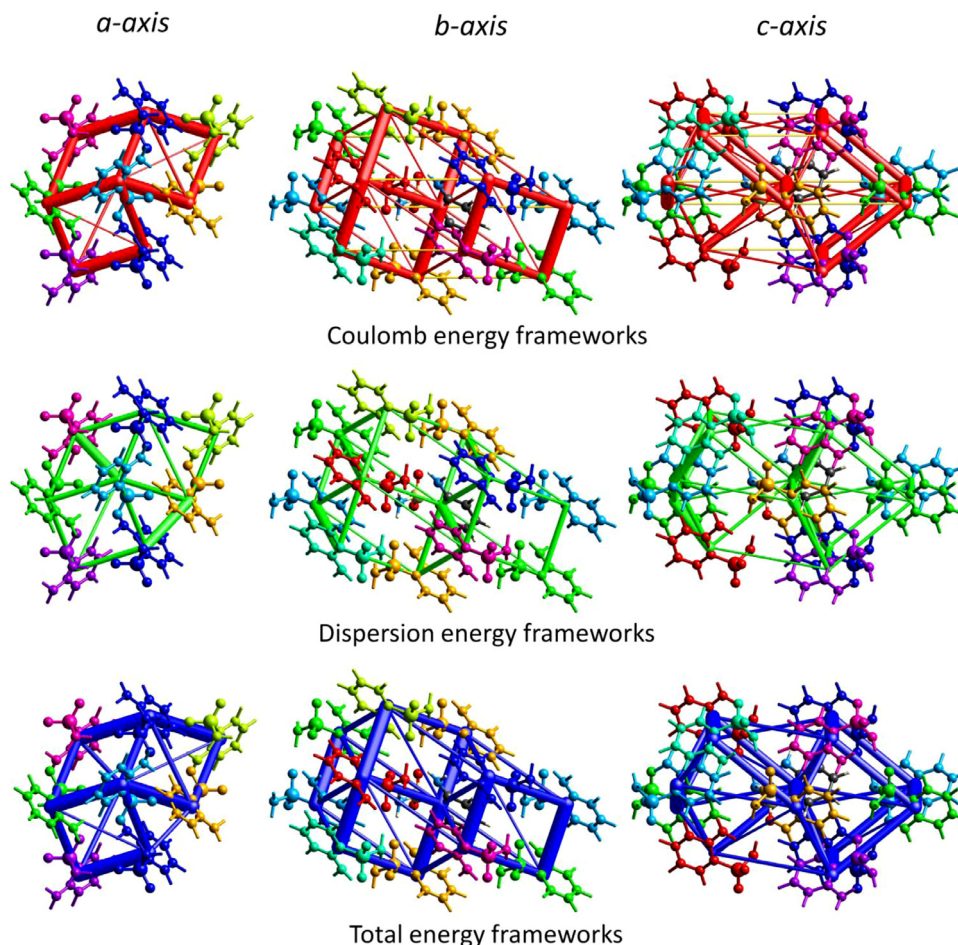


Fig. 5. The color-coded interaction energy framework of **9** viewed along the crystallographic *a*, *b* and *c* axes. Energy framework diagram for electrostatic, dispersion and total interaction energy. The energy factor scale is 100 and the cut-off is 5.00 kJ/mol.

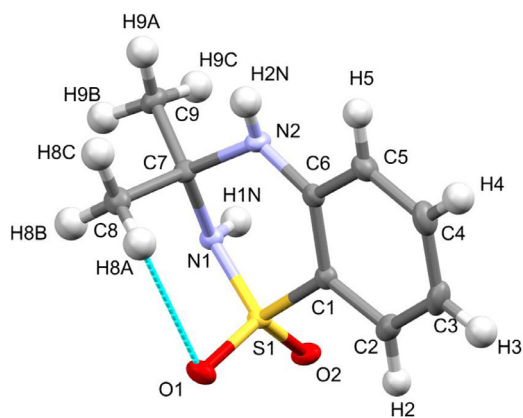


Fig. 6. The molecular structure of the title compound showing the atom labeling. Displacement ellipsoids are drawn at the 50% probability level. Intramolecular interaction C8–H8A...O1 is represented as dash cyan colored line.

plot identifying surface patches associated to different molecule-molecule close contacts possesses regions in green divided by blue boundaries. Therefore, $X-H\cdots\pi$ interaction is evidenced by the presence of a light blue point in the center of patches surrounded by yellow circle on the curvedness surface (Fig. 8).

In addition to the discussed contacts descriptors that could be mapped on Hirshfeld surfaces, the electrostatic potentials for the benzothiadiazine **10** were calculated at B3LYP/6–31G(d,p) level of

theory and mapped on the Hirshfeld surfaces (Fig. 8). The map analysis provides direct insight into intermolecular interactions in crystals and allows evaluation of the electron-rich and electron-deficient sites in the molecule. The blue and red regions around the different atoms correspond to positive and negative electrostatic potentials respectively. As shown in Fig. 8, the electronegative regions are essentially located around the oxygen atoms of the sulfonamide group and the electropositive regions were observed around the $N-H$ atoms.

Direct visualization of electrostatic potential isosurface allows a good observation of electron cloud which covers all atoms of compound **10**. Electrostatic potential isosurface (0.08 au) shown in Fig. 9a highlight that the clouds colored in red are mainly located over oxygen atoms of the sulfonamide group and are slightly larger than that of other atoms. This is due to the high electronegativity of oxygen. The perturbation of the electrostatic potential isosurface induced by neighboring molecules can be understood thanks to the deformation density surface analysis. The deformation density defined as the difference between the total electron density of a molecule and the electron density of *neutral spherical unperturbed atoms* superimposed at the same atomic positions of the molecule [44,45] is calculated at an isovalue of 0.008 to -0.008 a.u. The wave function was calculated at B3LYP/6–31G(d,p) level of theory embodied in CrystalExplorer17. The representation of the deformation density of 3,3-dimethyl-3,4-dihydro-2H-1,2,4-benzothiadiazine 1,1-dioxide (**10**) is shown in Fig. 9b. This figure displays blue (positive) and red (negative) isosurfaces of the deformation electron density which correspond to local increases and

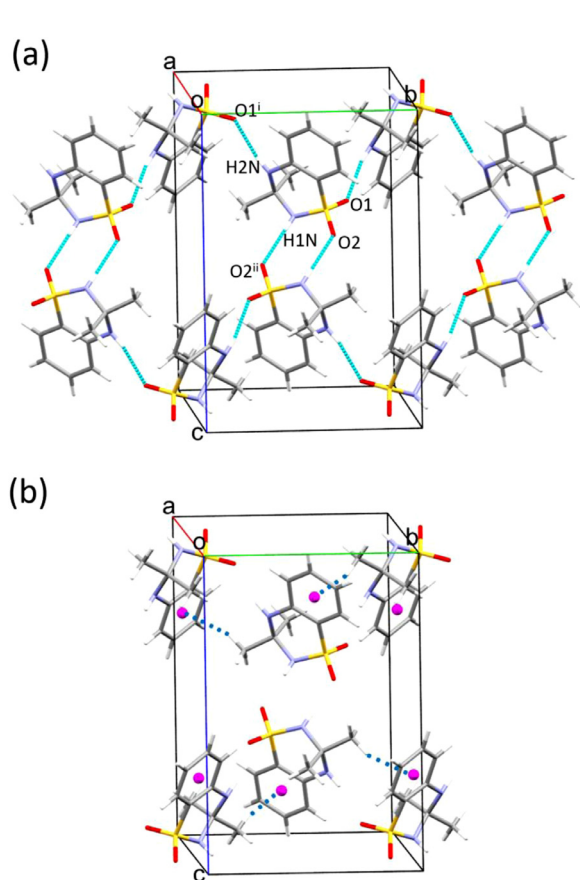


Fig. 7. (a) Intermolecular interactions in the crystal packing of title compound. Symmetry codes: (i) $-x + 1/2, y + 1/2, -z + 3/2$; (ii) $-x + 1, -y + 1, -z + 1$. (b) View of the intermolecular $X-H\cdots\pi$ interactions in the crystal packing.

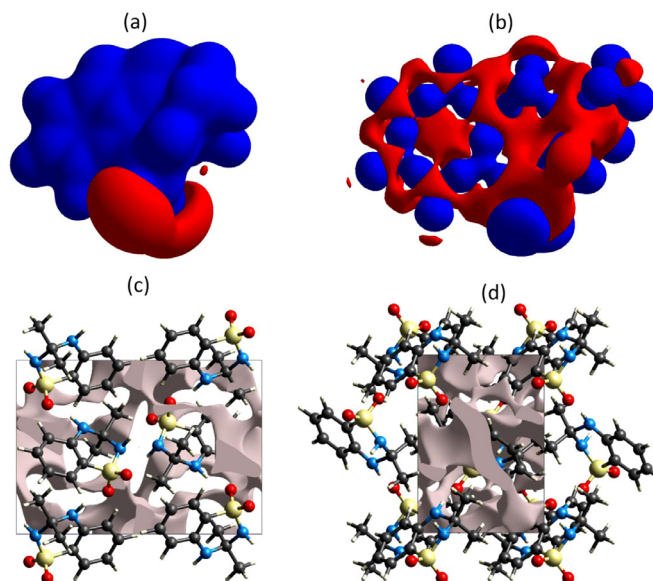


Fig. 9. Graphical representation of electrostatic potential isosurface (a), deformation electron density (b) and view along a (c) and c (d) crystallographic axis of crystal voids of compound **10**.

decreases, respectively, of electron density relative to the sum of spherical atoms. The deformation electron density observed around the aromatic ring is typical of those observed for the benzene ring [46]. In the thiaziazine ring, the presence of prominent blue domains around the oxygen atoms reveal notable increases of the electron density. This result can be explained by the fact that these oxygen atoms are implicated in hydrogen bonds as depicted on Hirshfeld surface mapped over d_i and Shape index as acceptor groups. On the contrary, a small deficit of electron density is observed around the N atoms. This plot shows clearly how the crys-

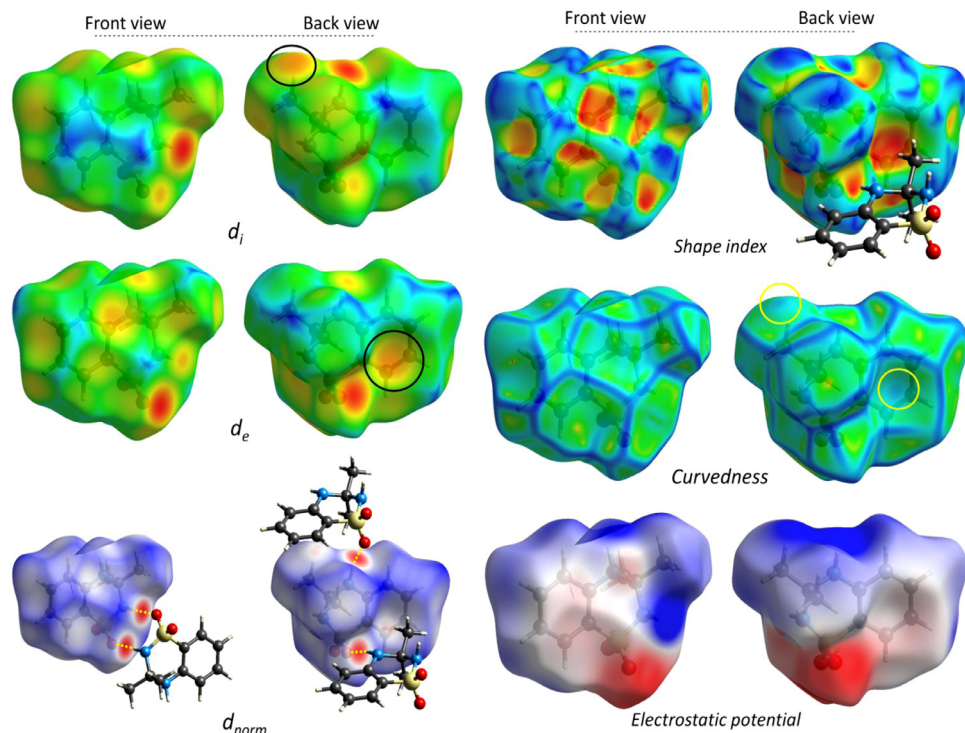


Fig. 8. The Hirshfeld surface of compound **10** mapped over d_i in the range 0.7814 to 2.5979 Å, d_e in the range 0.7830 to 2.5516 Å, d_{norm} in the range -0.5418 to 1.4079, Shape index (-1 to $+1$), curvedness (-4 to $+4$) and electrostatic potential (-0.0819 to 0.0522 a.u.).

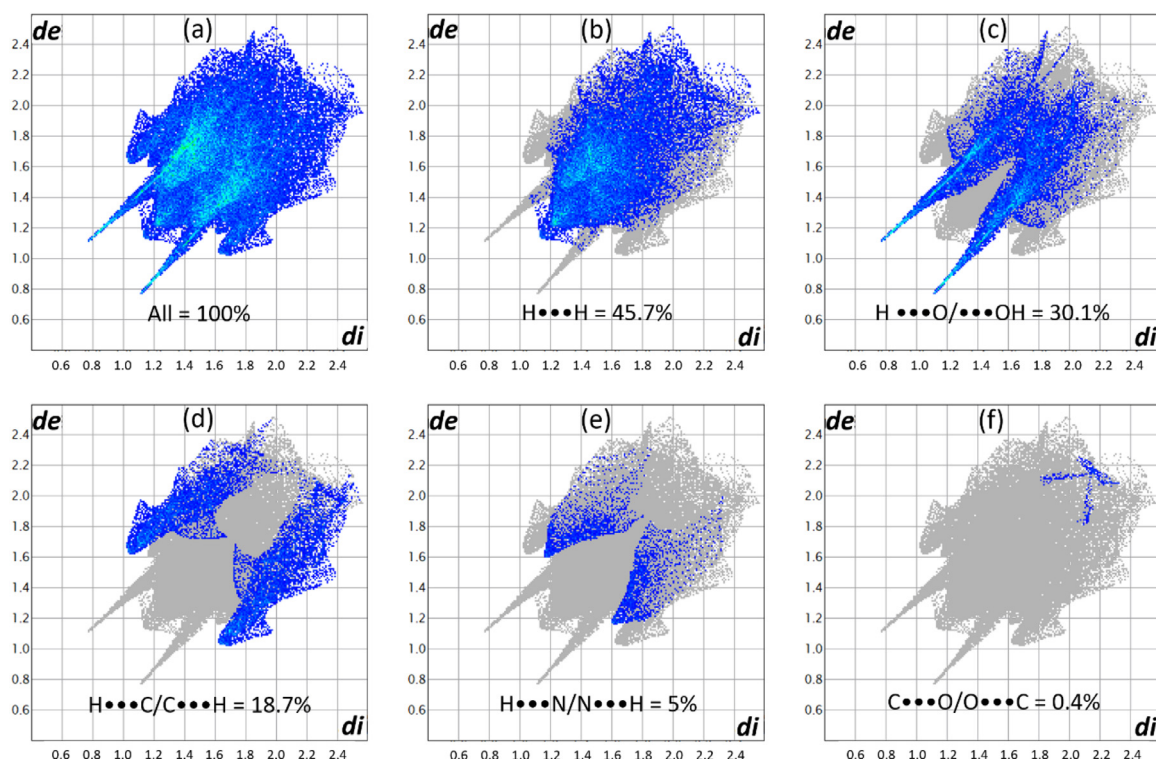


Fig. 10. Two dimensional fingerprint plot of the benzothiadiazine **10**. (a) All interactions, and (b) $H\cdots H$, (c) $H\cdots O/O\cdots H$, (d) $H\cdots C/C\cdots H$, (e) $H\cdots N/N\cdots H$ and (f) $C\cdots O/O\cdots C$ interactions.

tallographic environment can modify the electron density of the surrounding molecules.

The various contacts can also be described by considering the voids in crystalline materials [47]. The crystal packing is mainly governed by the existence of weak and strong interactions leading to the presence of voids in the crystal material. Therefore, the presence of hydrogen bonds as well as $X-H\cdots\pi$ interactions stabilizing the crystal packing of compound **10** reduce connected voids throughout the material. Fig. 9c and d show a view along *a* and *c* crystallographic axis of crystal voids present in **10** to allow better visualization of interconnected voids. Calculations gave void volume of 120.90 \AA^3 , an area of 391.28 \AA^2 , a globularity of 0.302 and asphericity value of 0.161.

The contacts at the origin of the deformation electron density and those with less influence are depicted in the two-dimensional fingerprint plot of the benzothiadiazine (Fig. 10). The fingerprint of **10** is almost similar to that of **9**. Nevertheless, the decomposed interactions are totally different. The presence of two methyl groups substituted on the thiadiazine ring enhances the $H\cdots H$ contact with a percentage of 45.7%. The $H\cdots O/O\cdots H$ interaction (30.1%) is the second important interaction thanks to the presence of different hydrogen bonds. Together with these two contacts, the $X-H\cdots\pi$ depicted as $H\cdots C/C\cdots H$ (18.7%) interactions, account for 94.5% of the overall interactions. Two less important contributions corresponding to $H\cdots N/N\cdots H$ and $C\cdots O/O\cdots C$ contacts are also observed (Fig. 10).

In addition to describing the 3D-topology of the predominant interactions, the shearing/bending properties, the mechanical properties, it was proven that energy frameworks play important role in intermolecular interactions even in liquids [48]. All the interactions are then quantified by computing the energy that stabilizes the crystal packing. The graphical representation of Coulomb interaction energy (red), dispersion energy (green) and total interaction energy (blue) of the compound **10** viewed down *a*, *b*, and *c* axes are presented in Fig. 11. Table S3 shows information about

interaction energies components (*E*), rotational symmetry operations with respect to the reference molecule (Symop), the centroid-to-centroid distance between the reference molecule and interacting molecules (*R*) as well as the number of pair(s) of interacting molecules with respect to the reference molecule (*N*). Furthermore, the scale factors (k_{ele} , k_{dis} , k_{pol} and k_{rep}) for total energies are also reported for two benchmarked energy models of electron density functions CE-HF/3-21 G and CE-B3LYP/6-31G(d,p) (Table S3).

The computed interaction energies for electrostatic, polarization, dispersion, and exchange repulsion are -133.2 kJ/mol , -39.8 kJ/mol , -140.2 kJ/mol , and 163.2 kJ/mol respectively. The dispersion energy and electrostatic energy values are in the same order with the first component slightly higher. A total interaction energy of -192 kJ/mol was obtained.

3.2.5. Non-covalent interaction (NCI) analysis of compound **10**

The interactions in the crystal packing discussed above are also examined using the non-covalent interactions (NCI) according to the procedure developed by Johnson and coworkers [49]. The reduced density gradient (RDG) is a dimensionless quantity obtained by the relation $\text{RDG}(r) = 12(3\pi r^2)^{1/3}|\nabla\rho(r)|\rho(r)^{4/3}$, is plotted against the electron density ρ to give the molecular interaction strength. On the RDG isosurface map, the region colored in blue indicates the presence of strong interaction whereas, green and red regions attests the presence of low and strong repulsion forces respectively (Fig. 12). The results were obtained using Multiwfn software [50] and VMD application [51], respectively.

Result presented in Fig. 12 shows the calculated isosurface of the BTd. The blue colored isosurfaces observed between $N-H\cdots O$ atoms reveal the presence of strong interaction confirming therefore the existence of hydrogen bonds described above. Furthermore, the green-blue light colored isosurface observed between one hydrogen of the methyl group and the neighboring phenyl ring shows Van der Waals-type interaction attested the $X-H\cdots\pi$ interactions discussed earlier. Finally, the red colored ovals isosurfaces

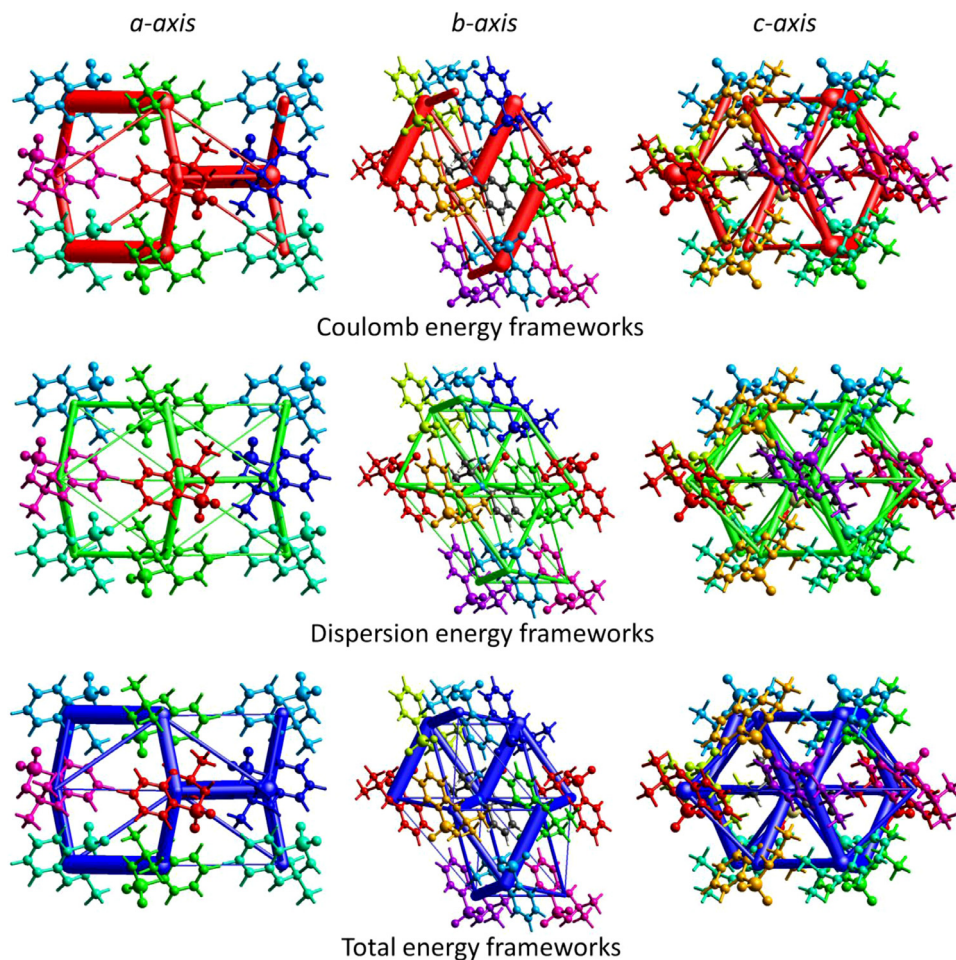


Fig. 11. Energy frameworks corresponding to the different energy components and the total interaction energy along *a*, *b* and *c* axis. The energy factor scale is 100 and the cut-off is 5.00 kJ/mol.

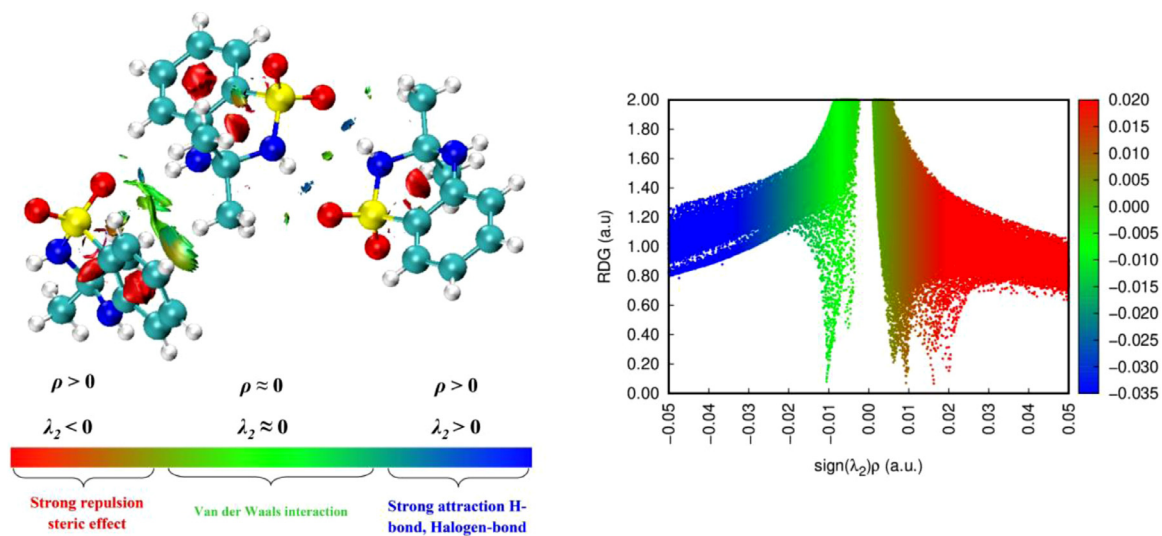


Fig. 12. Non-covalent interaction diagram (left) and reduced density gradient scatter plot (right) for the title molecule.

Table 3

OSIRIS calculations of toxicity risks of compounds **3**, **9** and **10**. DL: Drug likeness, commercial drugs found that about 80% of the known drugs had positive values of the Drug Likeness parameter, while almost all of the non-druglike chemicals had negative values. A positive value of Drug Likeness indicates that the molecule consists mostly of building fragments that are commonly found in commercial drugs. DS: Drug-Score. DS value of 1.0–0.8 (no risk), 0.8–0.6 (medium risk) and <0.6 (high risk).

Compound	MW	Toxicity Risks				OSIRIS calculations				
		Mutagenic	Tumorigenic	Irritant	Reproductive effective	LogP	TPSA	LogS	DL	DS
3	242.28	+++	+++	+++	+++	1.24	57.79	-2.96	1.42	0.82
9	172.21	+++	+++	+++	+++	-0.25	94.56	-0.59	-1.94	0.55
10	212.27	+++	+++	+++	+++	0.87	66.58	-1.94	2.71	0.93

MW: molecular weight (<500).

Highly toxic: (-), slightly toxic: (+), Not toxic (+++).

TPSA: total molecular polar surface area (no greater than 140 Å²).

LogP: the logarithm of the octanol-water partition coefficient of the compound (<5).

LogS: the logarithm of aqueous solubility (-6.5 to 0.5).

observed in the center of the rings are attributed to strong repulsion forces resulting from steric effect.

3.3. Physicochemical description

The physicochemical analysis is important to evaluate drug-like candidates [52]. For this goal, OSIRIS Property Explorer program of organic portal [53] was used to predict various physicochemical parameters and the values are given in Table 3. For a well-recognized AMPARpam **3** [12], physicochemical parameters were also obtained and compared to those obtained for the new BTM **10** and the sulfonamide **9**.

The toxicity risk values prediction obtained from OSIRIS software revealed that the three compounds (**3**, **9** and **10**) are expected not to display mutagenic, tumorigenic and irritant properties. Good oral bioavailability of drug depends strongly on the appropriate balance between hydrophilicity and lipophilicity. High hydrophobicity is associated with high LogP value. In addition, according to the Lipinski's rule of five [54], for a selected compound, a LogP value lower than 5.0 and a molecular weight lower than 500 are expected to warrant a possible oral bioavailability. With a molecular weight lower than 500 and a low value of LogP (0.87), compound **10** has a good oral absorption probability. A low total molecular polar surface area TPSA (Table 3) is obtained for the three compounds. OSIRIS combines the values of LogP, LogS, MW, DL, and toxicity risks in a single value named Drug Score used to evaluate the compound's overall drug potential. With a DS of 0.93, and DL of 2.71, compound **10** is expected to become a real potential drug candidate. The definition of "drug-like" was further refined to give "lead-like" to better describe the drugs candidates properties [55]. Such definition suggests for the small molecule that in addition of a rule of five, MW < 300, the LogP < 3, the H-bond donors < 3 and rotatable bonds < 3 [56]. As shown in Tables 3 and with two H-bond donors, no rotatable bond, compound **10** satisfied all these conditions and could be considered as a "lead-like" drug.

3.4. Molecular docking study of compound **10**

The binding mode of the new BTM **10** at the level of the allosteric binding site of the GluA2-type AMPAR using computational docking study is explored since BTM are well known as AMPARpam. Depending on their chemical structures, their lipophilicity, and their steric properties, the modulators interact with the dimer interface of the LBD of the ionotropic glutamate receptor GluA2 (GluA2-LBD) in different manners.

Starting from the cocrystal structure of BPAM344 monomer with GluA2o-LBD-L504Y-N775S (PDB code 4N07, resolution of 1.87 Å) [11] obtained from the protein data bank, the docking calculations with **10** were performed. The ligand-binding domains

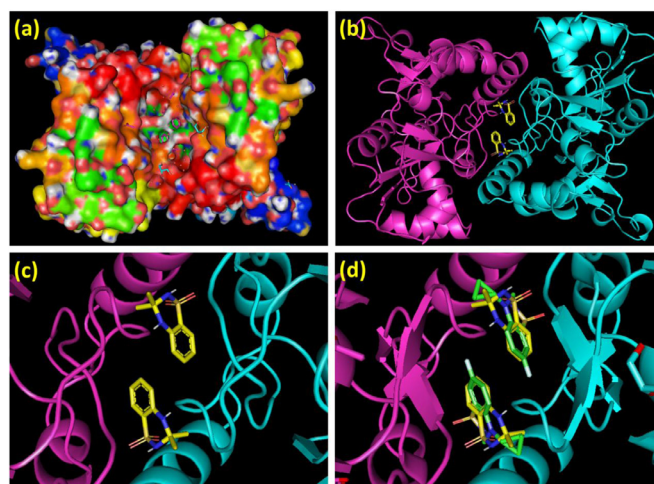


Fig. 13. (a) Docking result showing compound **10** (in magenta sticks) enclosed in the GluA2 active pocket. (b) Ribbon representation of the docked **10** (in yellow sticks) with GluA2. (c) Zoom on the modulator binding site containing two molecules of **10**. (d) Comparison of the domain occupancy of **10** and **3** showing that **10** (in yellow sticks) and **3** (in green sticks) occupy the same domain in the GluA2-LBD dimer interface.

(LBD) of GluA2 are well described thanks to crystallographic studies [14,57,58]. Docking compound **10** with the GluA2 and examination of the interactions at the region of the modulator binding site are expected to predict its activity. The molecular docking results showed that compound **10** binds to the allosteric binding site in the same region than other known BTM modulators like BPAM344 (**3**) [11] (Fig. 13a-c). The docking protocol was validated by re-docking compound **3** in GluA2 LBD. Superimposition of the 200 runs poses result is reported in Figure S6. 97% of the docking poses match with the experimental GluA2o-LBD-L504Y-N775S complex (Figure S6 and S7). Validation of the docking shows that rigid body approach (See Supporting Information) gives satisfactory result. Compound **10** interacts with the B and C subsites of the GluA2 LBD in a symmetrical way leading to an interaction of one molecule per subunit, and resulting in the binding of two molecules of **10** at the dimer interface as previously observed with BPAM344 (Fig. 13b-c) [11]. As shown in Fig. 13d, superimposition of the structure of compounds **10** and **3** in the LBD shows a slight rotation and therefore a displacement of the thiaziazine ring of **10** compared to **3** leading to the superimposition of the two methyl groups of **10** with the cyclopropyl group of **3**.

The active pocket of GluA2 containing the title compound is surrounded by various amino acids as shown in Fig. 14a. These residues can interact with the docked molecule by forming hydrogen bonds (HBs) or $\pi \cdots \pi$ short contacts. The zoom in of the

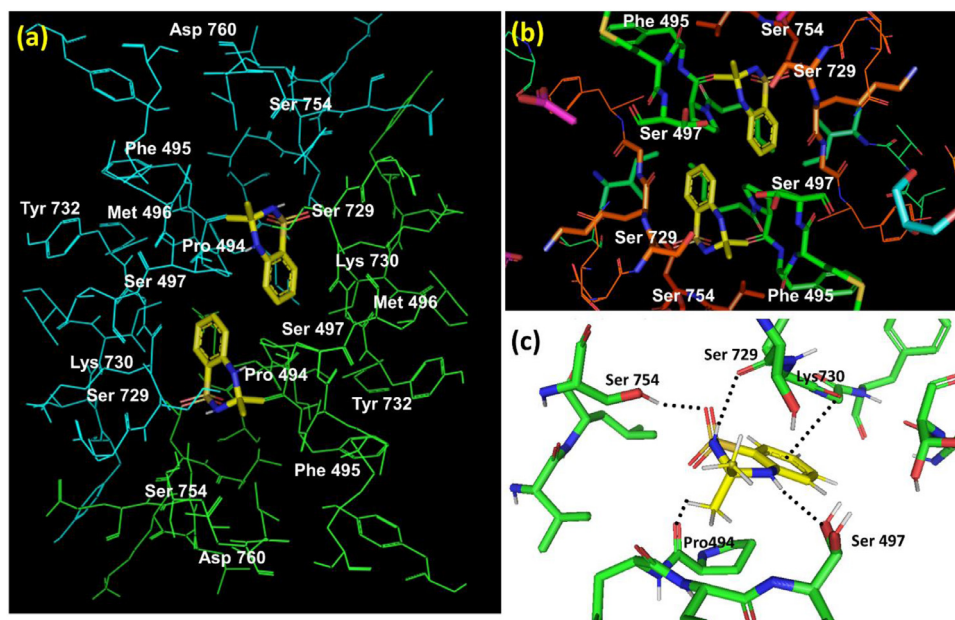


Fig. 14. (a) Active pocket showing the amino acids residues surrounded the GluA2-LBD containing compound **10**. (b) Zoom in of the amino acids that could interact with the docked molecule and (c) probable interactions of the residues surrounding compound **10** highlighted as dash black dot lines.

LBD presented in Fig. 14b reveals that residues Ser497, Ser729 and Ser754 could easily form HBs with the docked compound. The deep analysis of the binding mode revealed that compound **10** could form different HBs highlighted as black dot lines and shown in Fig. 14c. Careful examination of the interactions shows that one oxygen atom of the sulfonamide group could be implicated in HB with the hydroxyl group of Ser754. The presence of two $N-H$ bonds at the 2- and 4-position of the benzothiadiazine ring could allow short interaction with carbonyl oxygen of the residues. Indeed, $N1H$ and $N2H$ hydrogen atoms are oriented toward residues Ser729 (2.1 Å) and Ser497 (2.4 Å) respectively, forming probably two more interactions. Other contact like Van der Waals interaction can be depicted between one methyl hydrogen of the target molecule with Pro494. In addition, an oxygen atom of the carbonyl group of Lys730 located above the phenyl cycle of compound **10** could lead to $\pi\cdots\pi$ interaction (Fig. 14c).

Parameters such as binding energy, inhibition constant and intermolecular energy of the ligand were also calculated. The best docked pose of compound **10** (as illustrated in Fig. 13) shows same binding and intermolecular energy of ~ -6.67 kcal.mol⁻¹, ligand efficiency ~ -0.57 and inhibition constant ~ 12.91 μ m. Comparison of binding mode of **3** and **10** in GluA2-LBD shown small differences but most of the same residues (Pro494, Ser497, Ser729 and Ser754) participate to the various interactions. Finally, the docking analysis suggests clearly that compound **10** can interact with the GluA2-LBD and therefore is a good candidate as AMPAR-PAM.

4. Conclusion

The synthesis and full characterization of a new BTd 3,3-dimethyl-3,4-dihydro-2H-1,2,4-benzothiadiazine 1,1-dioxide **10** was achieved and reported in this work. This novel compound was obtained by simple reaction at room temperature of 2-aminobenzenesulfonamide with acetone. The molecular structure of the BTd as well as its precursor were obtained by X-ray diffraction analysis. The interactions stabilizing the crystal structures were analyzed thanks to the mapping of various contact descriptors on the Hirshfeld surface. The electron donor and acceptor domains of compound **10** were identified using the electrostatic potential property mapped on the Hirshfeld surface. In addition,

the effect of the molecular environment was depicted and visualized on the electron density isosurface. The fingerprint plots analysis allows to distinguish the predominant contact stabilizing these crystal packing dominated by O \cdots H, H \cdots H and C \cdots H contacts in **9** and **10** respectively. As a new drug candidate, the physicochemical properties of the BTd **10** were predicted using OSIRIS. The values obtained allow to consider **10** as a lead-like drug. Finally, molecular docking results clearly showed that BTd **10** could easily enter GluA2 LBD, interacts with the LBD residues and could occupy the same binding site than the reference compound BPAM344: Furthermore, the presence of two methyl groups at the 3-position of the thiadiazine ring of **10** appeared to induce a low rotation of the ligand. As a result, these methyl groups could occupy almost the same position than the cyclopropyl group of BPAM344. These data are consistent with the fact that compound **10** could be a new kind of AMPAR-PAM. Other new BTds are currently prepared in view to elucidate the structure/activity relationship. This study will be confirmed by pharmacological in vitro testing that can definitively conclude on the activity of **10** as an AMPAR modulator.

Credit authorship contribution statement

Koffi Senam Etsè: Design; Investigation; Conceptualization; Data curation; Formal analysis; Writing - original draft; Writing - review & editing

Guillermo Zaragoza: Data curation, Crystal data collection and analysis

Kodjo Djidjolé Etsè: Data curation; Formal analysis.

Declaration of Competing Interest

The authors declare that there are no conflicts of interest regarding the publication of this article.

Acknowledgements

This research did not receive any specific grant from funding agencies in the public, commercial, or not-for-profit sectors.

Supplementary materials

Supplementary material associated with this article can be found, in the online version, at doi:10.1016/j.molstruc.2021.130435.

References

- [1] T.V.P. Bliss, G.L. Collingridge, Synaptic model of memory: long-term potentiation in the hippocampus, *Nature* 361 (1993) 31–39.
- [2] J.M. Henley, K.A. Wilkinson, Synaptic AMPA receptor composition in development, plasticity and disease, *Nat. Rev. Neurosci.* 17 (2016) 337–350.
- [3] J.C. Lauterborn, G. Lynch, P. Vanderklish, A. Arai, C.M. Gall, Positive modulation of AMPA receptors increases neurotrophin expression by hippocampal and cortical neurons, *J. Neurosci.* 20 (2000) 8–21.
- [4] N. Nagarajan, C. Quast, A.R. Boxall, M. Shahid, C. Rosenmund, Mechanism and impact of allosteric AMPA receptor modulation by the Ampakine CX546, *Neuropharmacology* 41 (2001) 650–663.
- [5] A.C. Arai, M. Kessler, G. Rodgers, G. Lynch, Effects of the Potent Ampakine CX614 on hippocampal and recombinant AMPA receptors: interactions with cyclothiazide and GYKI 52466, *Mol. Pharm.* 58 (2000) 802–813.
- [6] A.M. Weeks, J.E. Harms, K.M. Partin, M. Benveniste, Functional Insight into Development of Positive Allosteric Modulators of AMPA Receptors, *Neuropharmacology* 85 (2014) 57–66.
- [7] R. Jin, S. Clark, A.M. Weeks, J.T. Dudman, E. Gouaux, K.M. Partin, Mechanism of Positive Allosteric Modulators Acting on AMPA Receptors, *J. Neurosci.* 25 (2005) 9027–9036.
- [8] J.R. Meyerson, J. Kumar, S. Chittori, P. Rao, J. Pierson, A. Bartsaghi, M.L. Mayer, S. Subramaniam, Structural Mechanism of Glutamate Receptor Activation and Desensitization, *Nature* 514 (2014) 328–334.
- [9] M. Bertolino, M. Baraldi, C. Parenti, D. Braghiroli, M. DiBella, S. Vicini, E. Costa, Modulation of AMPA/kainate Receptors by Analogues of Diazoxide and Cyclothiazide in Thin Slices of Rat Hippocampus, *Receptors Channels* 1 (1993) 267–278.
- [10] B. Pirotte, P. Francotte, E. Goffin, P. de Tullio, AMPA Receptor Positive Allosteric Modulators: a Patent Review, *Expert Opin. Ther. Pat.* 2 (2013) 615–628.
- [11] A.B. Nørholm, P. Francotte, L. Olsen, C. Krintel, K. Frydenvang, E. Goffin, S. Challal, L. Danober, I. Botez-Pop, P. Lestage, B. Pirotte, J.S. Kastrop, Synthesis, pharmacological and structural characterization, and thermodynamic aspects of GluA2-positive allosteric modulators with a 3,4-dihydro-2H-1,2,4-benzothiadiazine 1,1-dioxide scaffold, *J. Med. Chem.* 56 (2013) 8736–8745.
- [12] P. Francotte, E. Goffin, P. Fraikin, P. Lestage, J.C. Van Heugen, F. Gillotin, L. Danober, J.Y. Thomas, P. Chiap, A. Caignard, B. Pirotte, P. de Tullio, New fluorinated 1,2,4-benzothiadiazine 1,1-dioxides: discovery of an orally active cognitive enhancer acting through potentiation of the 2-amino-3-(3-hydroxy-5-methylisoxazol-4-yl)propionic acid receptors, *J. Med. Chem.* 53 (2010) 1700–1711.
- [13] E. Goffin, T. Drapier, A.P. Larsen, P. Geubelle, C.P. Ptak, S. Laulumaa, K. Rovinskaja, J. Gilissen, P. de Tullio, L. Olsen, K. Frydenvang, B. Pirotte, J. Hanson, R.E. Oswald, J.S. Kastrop, P. Francotte, 7-Phenoxy-Substituted 3,4-Dihydro-2H-1,2,4-benzothiadiazine 1,1-Dioxides as Positive Allosteric Modulators of α -Amino-3-hydroxy-5-methyl-4-isoxazolepropionic Acid (AMPA) Receptors with Nanomolar Potency, *J. Med. Chem.* 61 (2018) 251–264.
- [14] T. Drapier, P. Geubelle, C. Bouckaert, L. Nielsen, S. Laulumaa, E. Goffin, S. Dilly, P. Francotte, J. Hanson, L. Pochet, J.S. Kastrop, B. Pirotte, Enhancing Action of Positive Allosteric Modulators through the Design of Dimeric Compounds, *J. Med. Chem.* 61 (2018) 5279–5291.
- [15] D. Phillips, J. Sonnenberg, A.C. Arai, R. Vaswani, P. OKrutzik, T. Kleisli, M. Kessler, R. Granger, G. Lynch, A.R. Chamberlin, 5'-Alkyl-benzothiadiazides: a New Subgroup of AMPA Receptor Modulators with Improved Affinity, *Bioorg. Med. Chem.* 10 (2002) 1229–1248.
- [16] P.P. Shinoj Kumar, P.A. Suchetan, S. Sreenivasa, S. Naveen, N.K. Lokanath, D.B. Aruna Kumara, Crystal structure of (R)-6'-bromo-3,3-dimethyl-3',4'-dihydro-2'H-spiro[cyclohexane-1,3'-1,2,4-benzothiadiazine] 1',1'-dioxide, *Acta Cryst E70* (2014) 359–361.
- [17] S. Liu, J. Bao, X. Lao, H. Zheng, Novel 3D Structure Based Model for Activity Prediction and Design of Antimicrobial Peptides, *Sci. Rep.* 8 (2018) 11189.
- [18] K.-Z. Myint, L. Wang, Q. Tong, X.-Q. Xie, Molecular fingerprint-based artificial neural networks QSAR for ligand biological activity predictions, *Mol. Pharmaceutics* 9 (2012) 2912–2923.
- [19] M.B. Fernandes, M.T. Scotti, M.J.P. Ferreira, V.P. Emerenciano, Use of self-organizing maps and molecular descriptors to predict the cytotoxic activity of sesquiterpene lactones, *Eur. J. Med. Chem.* 43 (2008) 2197–2205.
- [20] G.R. Fulmer, A.J.M. Miller, N.H. Sherden, H.E. Gottlieb, A. Nudelman, B.M. Stoltz, J.E. Bercaw, K.I. Goldberg, NMR chemical shifts of trace impurities: common laboratory solvents, organics, and gases in deuterated solvents relevant to the organometallic chemist, *Organometallics* 29 (2010) 2176–2179.
- [21] Y. Girard, J.G. Atkinson, J.A. Rokach, New Synthesis of 1,2,4-Benzothiadiazines and a Selective Preparation of o-Aminobenzenesulphonamides, *J. Chem. Soc., Perkin Trans. 1* (1979) 1043–1047.
- [22] K.S. Etsè, L. Cameron Lamela, G. Zaragoza, B. Pirotte, Synthesis, crystal structure, Hirshfeld surface and interaction energies analysis of 5-methyl-1,3-bis(3-nitrobenzyl)pyrimidine-2,4,6-trione, *Eur. J. Chem.* 11 (2020) 91–99.
- [23] Bruker APEX II Bruker AXS Inc., Madison, WI, USA, 2004.
- [24] G.M. Sheldrick, SHELXT—Integrated space-group and crystal-structure determination, *Acta Cryst. A* 71 (2015) 3–8.
- [25] G.M. Sheldrick, PLATON SQUEEZE: a tool for the calculation of the disordered solvent contribution to the calculated structure factors, *Acta Cryst. C* 71 (2015) 3–8.
- [26] L.J. Farrugia, WinGX and ORTEP for Windows: an update, *J. Appl. Cryst.* 45 (2012) 849–854.
- [27] C.F. Macrae, I.J. Bruno, J.A. Chisholm, P.R. Edgington, P. McCabe, E. Pidcock, L. Rodriguez-Monge, R. Taylor, J. Van de Streek, P.A. Wood, Mercury CSD 2.0—new features for the visualization and investigation of crystal structures, *J. Appl. Cryst.* 41 (2008) 466–470.
- [28] G.M. Morris, R. Huey, W. Lindstrom, M.F. Sanner, R.K. Belew, D.S. Goodsell, A.J. Olson, AutoDock4 and AutoDockTools4: automated docking with selective receptor flexibility, *J. Comput. Chem.* 30 (2009) 2785–2791.
- [29] W.L. DeLano, PyMOL DeLanoScientific, 700, San Carlos, CA, 2002.
- [30] P.P. Shinoj Kumar, P.A. Suchetan, S. Sreenivasa, S. Naveen, N.K. Lokanath, D.B. Aruna Kumara, Crystal structure of (R)-6'-bromo-3,3-dimethyl-3',4'-dihydro-2'H-spiro[cyclohexane-1,3'-1,2,4-benzothiadiazine] 1',1'-dioxide, *Acta Cryst. E70* (2014) 359–361.
- [31] K.S. Etsè, G. Zaragoza, B. Pirotte, Crystal structure and Hirshfeld surface analysis of N-(2-(N-methylsulfamoyl)phenyl)formamide: degradation product of 2-methyl-2H-1,2,4-benzothiadiazine 1,1-dioxide, *Eur. J. Chem.* 10 (2019) 189–194.
- [32] K.S. Etsè, B. Dassonneville, G. Zaragoza, A. Demonceau, One-pot, Pd/Cu-catalysed synthesis of alkynyl-substituted 3-ylidenedihydrobenzo[d]isothiazole 1,1-dioxides, *Tet. Lett.* 58 (2017) 789–793.
- [33] M.J. Turner, J.J. McKinnon, S.K. Wolff, D.J. Grimwood, P.R. Spackman, D. Jayatilaka, M.A. Spackman, Crystal Explorer, 17, The University of Western Australia, 2017 <http://hirshfeldsurface.net>.
- [34] M.A. Spackman, D. Jayatilaka, *CrystEngComm* 11 (2009) 19–32.
- [35] J.J. McKinnon, M.A. Spackman, A.S. Mitchell, Novel tools for visualizing and exploring intermolecular interactions in molecular crystals, *Acta Cryst. B* 60 (2004) 627–668.
- [36] M.A. Spackman, J.J. McKinnon, Fingerprinting Intermolecular Interactions in Molecular Crystals, *CrystEngComm* 4 (2002) 378–392.
- [37] J.J. McKinnon, D. Jayatilaka, M.A. Spackman, Towards quantitative analysis of intermolecular interactions with Hirshfeld surfaces, *Chem Commun.* (2007) 3814–3816.
- [38] M.J. Turner, S.P. Thomas, M.W. Shi, D. Jayatilaka, M.A. Spackman, Energy frameworks: insights into interaction anisotropy and the mechanical properties of molecular crystals, *Chem. Commun.* 51 (2015) 3735–3738.
- [39] M.J. Turner, S. Grabowsky, D. Jayatilaka, M.A. Spackman, Accurate and efficient model energies for exploring intermolecular interactions in molecular crystals, *J. Phys. Chem. Lett.* 5 (2014) 4249–4255.
- [40] C.F. Mackenzie, P.R. Spackman, D. Jayatilaka, M.A. Spackman, CrystalExplorer model energies and energy frameworks: extension to metal coordination compounds, organic salts, solvates and open-shell systems, *IUCr* 4 (2017) 575–587.
- [41] S.L. Tan, M.M. Jotani, E.R.T. Tiekink, Utilizing Hirshfeld surface calculations, non-covalent inter-action (NCI) plots and the calculation of inter-action energies in the analysis of molecular packing, *Acta Cryst E75* (2019) 308–318.
- [42] D. Cremer, J.A. Pople, General definition of ring puckering coordinates, *J. Am. Chem. Soc.* 97 (1975) 1354–1358.
- [43] J.F. Malone, C.M. Murray, M.H. Charlton, R. Docherty, A.J. Lavery, X-H π (phenyl) interactions: theoretical and crystallographic observations, *J. Chem. Soc. Faraday Trans.* 93 (1997) 3429–3436.
- [44] W.H.E. Schwarz, K. Ruedenberg, L. Mensching, Chemical deformation densities. 1. Principles and formulation of quantitative determination, *J. Am. Chem. Soc.* 111 (1989) 6926–6933.
- [45] V. Meenatchi, S.P. Meenakshisundaram, Synthesis, growth, spectral studies, first-order molecular hyperpolarizability and Hirshfeld surface analysis of isonicotinohydrazide single crystals, *RSC Adv.* 5 (2015) 64180–64191.
- [46] A.J. Edwards, C.F. Mackenzie, P.R. Spackman, D. Jayatilaka, M.A. Spackman, Intermolecular interactions in molecular crystals: what's in a name? *Faraday Discuss* 203 (2017) 93–112.
- [47] M.J. Turner, J.J. McKinnon, D. Jayatilaka, M.A. Spackman, Visualisation and characterisation of voids in crystalline materials, *CrystEngComm* 13 (2011) 1804–1813.
- [48] S.P. Thomas, R. Sathishkumar, T.N. Guru Row, Organic alloys of room temperature liquids thiophenol and selenophenol, *Chem. Commun.* 51 (2015) 14255–14258.
- [49] E.R. Johnson, S. Keinan, P. Mori-Sanchez, J. Contreras-García, A.J. Cohen, W. Yang, Revealing non covalent interactions, *J. Am. Chem. Soc.* 132 (2010) 6498–6506.
- [50] T. Lu, F. Chen, Multiwfn: a multifunctional wavefunction analyzer, *J. Comput. Chem.* 33 (2011) 580–592.
- [51] W. Humphrey, A. Dalke, K. Schulten, VMD: visual molecular dynamics, *J. Mol. Graph.* 14 (1996) 33–38.
- [52] Y.N. Mabkhout, F. Alati, N. El-sayed, S. Al-Showman, N. Kheder, A. Wadood, A. Rauf, S. Bawazeer, T. Ben B. Hadda, Antimicrobial activity of some novel armed thiophene derivatives and petra/osiris/molinspiration (POM) analyses, *Molecules* 21 (2016) 222–238.
- [53] Organic Chemistry Portal. 2012. Available at <http://www.organic-chemistry.org/prog/peo/>.
- [54] C.A. Lipinski, F. Lombardo, B.W. Dominy, P.J. Feeney, Experimental and computational approaches to estimate solubility and permeability in drug discovery and development settings, *Adv. Drug Deliv. Rev.* 46 (2001) 3–26.

- [55] T.I. Oprea, A.M. Davis, S.J. Teague, P.D. Leeson, Is there a difference between leads and drugs? A historical perspective, *J. Chem. Inf. Comput. Sci.* 41 (2001) 1308–1315.
- [56] M. Congreve, R. Carr, C. Murray, H. Jhoti, A 'rule of three' for fragment-based lead discovery? *Drug Discov. Today* 8 (2003) 876–877.
- [57] A.P. Larsen, P. Francotte, K. Frydenvang, D. Tapken, E. Goffin, P. Fraikin, D.H. Caignard, P. Lestage, L. Danober, B. Pirotte, J.S. Kastrop, Synthesis and Pharmacology of Mono-, Di-, and Trialkyl-Substituted 7-Chloro-3,4-dihydro-2H-1,2,4-benzothiadiazine 1,1-Dioxides Combined with X-ray Structure Analysis to Understand the Unexpected Structure-Activity Relationship at AMPA Receptors, *ACS Chem. Neurosci.* 7 (2016) 378–390.
- [58] C. Krintel, P. Francotte, D.S. Pickering, L. Juknaitė, J. Pøhlsgaard, L. Olsen, K. Frydenvang, E. Goffin, B. Pirotte, J.S. Kastrop, Enthalpy-Entropy Compensation in the Binding of Modulators at Ionotropic Glutamate Receptor GluA2, *Biophys. J.* 110 (2016) 2397–2406.